Embers, Wind, and Fire: An investigation of the effects of embers and wind on wildfire propagation

Ananthajit ("Ananth") Srikanth and Jasmine Tai
Department of Applied Mathematics, University of California Santa Cruz

March 29, 2024

Abstract

Wildfires are recurring phenomena that present significant threats to human lives and infrastructure when left uncontrolled. In order to enact preventative measures, it is therefore crucial to thoroughly understand the various environmental factors that control their spread. In this paper, we focus on the study of ember and wind forces as they relate to wildfire propagation, analyzing how varying ember densities and cooling rates, as well as wind magnitudes, impact the rate and affected area of wildfire propagation in environments that are typically unfavorable to such propagation. We achieve this by developing a numerical model for fire propagation that implements the effects of embers and wind with a specified ember density, ember cooling rate, wind magnitude, and wind direction. The simulations we produce with this model show that decreasing the ember cooling rate accelerates the rate of fire propagation in a radial manner, whereas increasing wind magnitude does so only in the wind direction. We furthermore demonstrate that embers and wind combined can increase the size of a propagated fire by factors of 10-30x. This effect highlights the importance of recognizing the role embers play in spreading fire when scattered by wind.

1 Introduction

Wildfires have long been known to society as a disastrous and recurring natural phenomenon. In recent years, rapid climate change has only added to the longevity and frequency of wildfires; as a result, an estimated 250,000–1.5 million acres of land are burnt annually in California [1]. Although certain conditions such as hot and dry weather can contribute to the likelihood of wildfire genesis, it is often difficult to pinpoint the time and place of such an event. Consequently, wildfires may not be noticed until they are large enough to present some risk of danger to civilization, at which point they become difficult to control. The immediate risk that a nearby wildfire poses to people, homes, and other infrastructure is substantial, hence it can incur hefty costs in terms of the loss of life and property.

Although the natural recurrence of wildfires is inevitable, the study of their propagation over time is essential to prevent their spread. Wildfire propagation is noticeably affected by a multitude of environmental factors, including—but not limited to—elevation changes, topographical features such as bodies of water and buildings, and weather conditions such as precipitation and wind. Wind, in particular, can exert a significant influence on wildfire propagation in that it can help carry a fire in a certain direction and replenish the surrounding oxygen supply supporting a fire. Understanding in detail the effects of wind on the behavior of wildfires enables us to be better prepared to combat their spread.

While it is apparent that wind can influence the spread of fires to adjacent plots of land by ground travel, it is also known that embers from existing fires have the potential to act as powerful fire starters [2]. An ember is defined as "a small glowing fragment from a fire", usually made of coal or wood [3]. Due to their airborne nature, embers can quickly cover large distances and are especially sensitive to wind patterns, although their capacity to start new fires is limited because they tend to easily lose heat to their surroundings. Nonetheless, embers are far from negligible when it comes to the genesis and spread of wildfires, and many notable fires such as the Marshall Fire in Boulder, Colorado and the Witch Fire in California have begun from embers [4, 5]. In the case of the latter fire, additional embers spawned by the wildfire were the primary cause of destruction for many homes. These examples

of real-world scenarios provide a convincing motivation for studying the role of embers in wildfire propagation.

In this paper, we seek to assess how changes in ember cooling rate and wind magnitude interact with each other to impact the rate of wildfire propagation and wildfire size over time, particularly within environments that are otherwise not highly conducive to such propagation. We also investigate the effects of other parameters such as ember density, ember temperature, and wind direction on wildfire propagation, albeit to a lesser extent. To this end, we first create a probabilistic model for fire propagation that accounts for the effects of embers and wind independently, as defined by a set of chosen parameters. We then consider a model that delineates their combined effects. We implement and run this model for varied choices of ember and wind properties to compare the individual and combined effects on wildfire propagation.

Section 2 discusses the mathematical model we construct for fire propagation, which partially depends on ember density, temperature, and cooling rate as well as wind magnitude and direction. Section 3 describes how we build the model numerically, and Section 4 summarizes our findings on how variations in the model parameters influence the rate and affected area of fire propagation. We conclude with a discussion of the implications of the results and limitations of our model in Section 5.

2 Model

We begin by introducing the theoretical basis for a model that propagates fire over time in the absence of embers and wind in Section 2.1. We expand on the basic model to incorporate the behavior of embers in Section 2.2, and we separately consider modifications to the probabilities of fire spread based on a given wind magnitude and direction in Section 2.3. We follow up with a discussion how to combine the influences of embers and wind to define an overall probability of fire propagation for the space around an existing fire in 2.4. Lastly, in preparation for studying the effects of embers and wind, we define a metric for analyzing the relative area of a fire in Section 2.5.

2.1 Basic fire propagation

Consider a two-dimensional square grid of cells that represents a land area. Whether each cell is on fire or not can be encoded in an $n \times n$ matrix M, where elements that correspond to cells on fire are assigned 1, and are assigned 0 otherwise. Each cell can then be referenced by a row index i and a column index j, and in all that follows, we allow each of these indices to begin at 1 such that $(1, 1)$ defines the cell in the top left corner of M.

We simulate fire propagation over time by evolving M over a series of t discrete time steps from an initial state $M = M_{init}$, as illustrated in Figure 1 for a simple 3×3 matrix. During a time step, each cell has a base probability p_0 of ignition from neighboring cells on fire via ground spread. In choosing a random selection of cells to ignite, we thus treat M as a finite cellular automaton.

(a) Initial state   (b) After one time step

Figure 1: Example of fire propagation in a 3×3 matrix for one time step, with columns and rows indicated along the top and left sides respectively in gray. In the initial state, only one fire is present at $(2, 2)$. After one time step, the fire has spread to neighboring cells $(2, 3)$ and $(3, 2)$ based on a probability p_0 of fire propagation.

Besides embers and wind, which will each be described shortly, no other environmental factors are

taken into account when computing the total probability of fire propagation. Furthermore, we assume that there is an infinite amount of fuel in each cell such that fires never go out once started. While unrealistic, these assumptions help to simplify the numerical modeling so that we can focus purely on our study of the effects of embers and wind on fire propagation.

Due to the probabilistic nature of fire propagation, it is more useful to study the average behavior of fire propagation than to study the behavior of isolated instances. Therefore, we aim to compute a matrix M_{mean} that summarizes the mean state of M over time for s simulations, choosing a sufficiently large s so as to provide a good view of the true mean behavior of fire propagation. The resulting matrix is helpful both for validating the behavior of our model later and for deriving general conclusions about the behavior of fire propagation based on the patterns observed across multiple simulations.

2.2   Embers

To simulate the effects of embers over time, we first assume that embers can travel a distance d in a single time step. d must be greater than $\sqrt{2}$ as the furthest cell adjacent to a fire (namely, a cell diagonally adjacent to a fire) has a Euclidean distance of $\sqrt{2}$ relative to that fire. Thus, we have that $\sqrt{2} < d \leq d_{max}$, where d_{max} is the maximum distance that an ember can travel from a source fire. We will define a particular choice of d_{max} shortly.

Given that embers cool down the further they travel, we introduce an ignition probability $f(d)$ that decreases for increasing values of d. Newton's law of cooling implies that temperature decays exponentially with time, so if we assume a constant rate of advection, it follows that $f(d)$ can be modelled with a decreasing exponential function. We also assume that the probability of any ember igniting a cell is related to its initial temperature, such that a hotter ember is more likely to start a fire. Thus, we define

$$f(d) = p_1 e^{\frac{1-d}{d_0}} \tag{1}$$

where p_1 is a chosen measure of ember density and temperature and d_0 is a parameter inversely related to the cooling rate of the embers. In essence, for larger d_0, there exists a non-negligible probability of ignition for longer distances. To simplify our computation, we choose to only consider embers that travel up to 5 cells away relative to an ignited cell, thus creating an 11×11 matrix of associated probabilities. It follows that the furthest distance an ember can travel in such a model is $d_{max} = 5\sqrt{2}$.

Notice that for distances less than $\sqrt{2}$, we have $f(d) = p_0$. Hence, we can define $f(d)$ as a piecewise function:

$$f(d) = \begin{cases} p_0, & 0 \leq d \leq \sqrt{2} \\ p_1 e^{\frac{1-d}{d_0}}, & \sqrt{2} < d \leq 5\sqrt{2} \end{cases} \tag{2}$$

Figure 2 showcases the effects of different choices of p_1 and d_0 on $f(d)$ over d. We see that increasing p_1 increases the ignition probability for low values of d, which correspond to embers near the source fire; doing so only scales the number of embers and their temperature distribution up, which does not affect $f(d)$ for distant embers greatly. Increasing d_0, on the other hand, allows for a thicker tail in the plot since embers cool more slowly, letting them travel further distances with a non-negligible $f(d)$.

2.3   Wind

Now, consider a wind that blows with magnitude w and direction θ in radians. We would like the wind to increase the probability of fire spread in the directions with an offset of less than $\frac{\pi}{2}$ from that of the wind. For instance, for a wind that has an angle of $\frac{\pi}{2}$, we expect it to increase the probability of fire propagation for the northwest and northeast directions along with that of the north direction. This effect reflects how the presence of wind causes flames to lean towards certain directions in real-world scenarios, leaving areas in these directions more likely to catch fire. We also assume that wind does not negatively affect the probability of fire propagation in directions that oppose the wind.

Based on w and θ, we can construct an 3×3 matrix representation W that summarizes the influence of wind on the overall probability of fire propagation. The center element of W at $(2, 2)$ represents a fire source in a 3×3 window. For each element $(i, j) \neq (2, 2)$, $W(i, j)$ is a factor that is additive on p_0, representing the effect of wind on that element. In cells that are well-aligned to the direction of wind, $W(i, j)$ is larger than in cells that are not. We require that $W(i, j)$ be non-negative and scaled so that, in general, $p_0 + W(i, j) \leq 1$ for our choices of w.
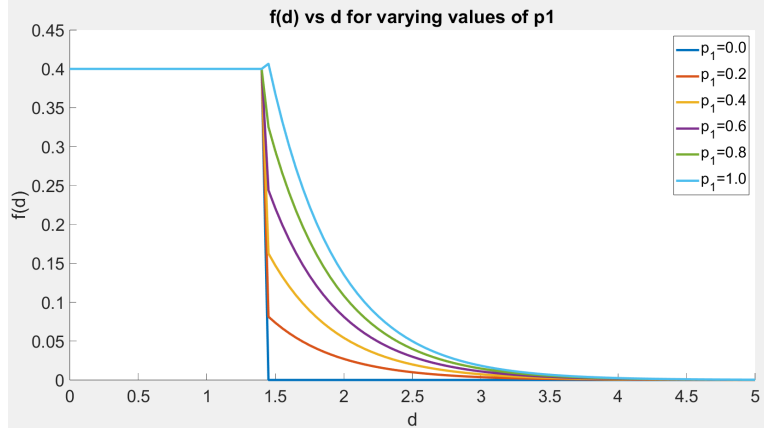
(a) $f(d)$ vs. d for various $p_1 \in [0, 1]$ and $d_0 = 0.5$
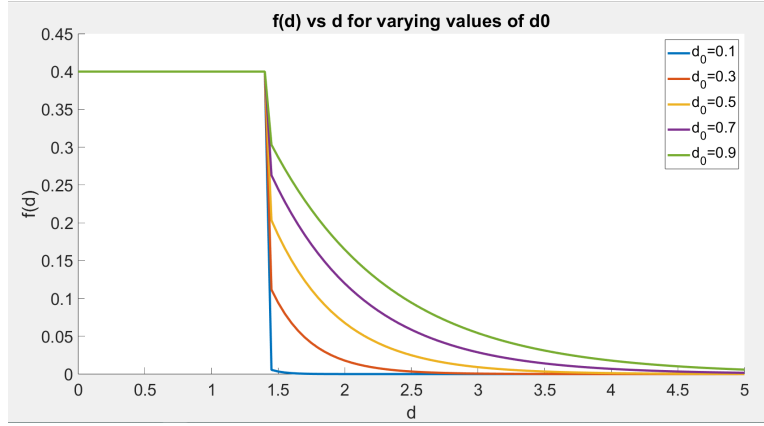
(b) $f(d)$ vs. d for various $d_0 \in [0, 1]$ and $p_1 = 0.5$

Figure 2: Comparison of $f(d)$ vs. d for various values of p_1 (2a) and various values of d_0 (2b). As p_1 increases, $f(d)$ primarily increases for embers **close** to the source fire and minimally affects distant embers. As d_0 increases, $f(d)$ primarily increases for embers **distant** from the fire (note the "tail" of $f(d)$) and noticeably increases for low d as well, but not to the same extent as when increasing p_1.

We now propose a means of determining $W(i, j)$ based on w, θ, and the indices (i, j) of each element. First, note that the wind vector defined by w and θ can be expressed in terms of Cartesian coordinates as $\boldsymbol{w_{xy}} = [w_x; w_y] = [w\cos(\theta); w\sin(\theta)]$. Each of the eight possible directions we consider in the 3×3 window for fire propagation can also be expressed as vectors $\boldsymbol{t_{ij}} = [t_{ijx}; t_{ijy}] = [j - 2; 2 - i]$, with $t_{ijx}, t_{ijy} \in \{-1, 0, 1\}$. Then, for each $\boldsymbol{t_{ij}}$, the associated $W(i, j)$ is determined as

$$W(i, j) = max \left(0, a \frac{(\boldsymbol{w_{xy}} \cdot \boldsymbol{t_{ij}})}{||\boldsymbol{t_{ij}}||} \right) \tag{3}$$

where a is a selected constant of proportionality for scaling $W(i, j)$ to a magnitude that is appropriately additive to $f(d)$. Thus, $W(i, j)$ is a value that varies proportionally to the magnitude of w and depends on how well-aligned the direction of fire propagation is to the wind direction θ. Using Eq. 3 on each (i, j) that surrounds $(2, 2)$ in W yields the representation of wind we need to determine the total probability of fire propagation based on both $f(d)$ (as defined in Equation 2) and the influence of wind.

2.4 Joint model

In each time step during the evolution of the cellular automaton M, we use $f(d)$ and W to compute the total probability of fire propagation along all possible directions of propagation from every ignited

4

cell. We can sum the influences of the ember and wind-based models in a combined matrix K such that

$$K(i,j) = f(d) + W(i,j) \qquad (4)$$

If we consider a cell on fire as the center of a 11×11 window in M, then the total probability of a fire spreading from that cell to a cell with relative indices (i,j) within the 11×11 window is

$$p_{ij} = max(0, min(1, b \cdot K(i,j))) \qquad (5)$$

where b is a random multiplicative factor within $[0.95, 1.05]$ applied to simulate small variations in wind and ember distribution over time and space that occur in real-world scenarios. To ensure that $0 \leq p_{ij} \leq 1$, we take the minimum of 1 and $b \cdot K(i,j)$ as well as the maximum of 0 and the found minimum. Additionally, to reflect the variations that occur over time in a realistic setting, we recompute all p_{ij} every time we construct a new 11×11 window around an ignited cell in each time step. Eq. 5 therefore generates slightly different probabilities to be used in each time step, while Eq. 4 gives the combined base influences of embers and wind that do not vary by time step.

2.5 Area analysis

As a baseline metric for comparing the areas of simulated fires, we use the average number of cells on fire after the last time step when $p_1 = 0$ and $w = 0$, which represents a situation in which the environment is devoid of embers and wind. c_b is thus defined as the sum of all entries in M_{mean}, and it can be computed relatively quickly for as many as $s = 1,000$ simulations. This is generally *not* the case when ember propagation and wind factors are taken into account, so for each pairing of d_0 and w, we prefer to calculate the average number of cells on fire c in M using fewer simulations. The quantities c_b and c then allow us to find the overall increase in area in the form of a ratio

$$r_c = \frac{c}{c_b} \qquad (6)$$

for a given d_0 and w, which will prove useful in studying the affected area of fire propagation.

3 Method

In what follows, we describe the numerical algorithm we developed to compute M_{mean} for a set of given input parameters. To begin with, the basic parameters are p_0, the base probability of fire propagation through ground travel; n, the size of the $n \times n$ matrix M; t, the number of time steps; s, the number of simulations; and M_{init}, the initial state of M. To implement embers, we additionally consider p_1, the measure of ember density and temperature referenced in Eq. 2, and d_0, a parameter inversely proportional to the ember cooling rate. To implement wind, we specify w, the wind magnitude; θ, the wind direction; and a, the constant of proportionality used in computing $W(i,j)$ in Eq. 3. Note that the equations we use allow us to consider scenarios without embers by setting p_1 to 0 and scenarios without wind by setting w to 0. This makes it simple to observe the effects of each influence separately when desired.

In order to run s simulations of the evolution of M over t time steps and save the results, we first need to define the matrices M_{mean} and K. We create the $t \times n \times n$ matrix M_{mean} to store the mean state of M over time across all simulations, initializing all values to zero. K is defined as an 11×11 kernel where $K(i,j)$, computed from Eq. 4, depends on the contributions of embers and wind through $f(d)$ and W. We loop over all elements in K, calculating both $\boldsymbol{t_{xy}}$ and the distance d, which is the norm of $\boldsymbol{t_{xy}}$. Then each $K(i,j)$ can be computed, where the relevant $f(d)$ is calculated based on Eq. 2 and the relevant $W(i,j)$ is calculated based on Eq. 3.

Once M_{mean} and K are initialized, we perform s simulations of the fire propagation in M. In each simulation, we model fire propagation in M for t time steps, beginning with $M = M_{init}$. In each time step, we pass a sliding 11×11 window through the current state of M to perform updates on individual cells and thereby build the new state of M. For each state of the window, if the center cell contains a fire, we update all of the surrounding cells within said window, using their indices (i,j) relative to the ignited cell to relate them to the associated p_{ij} calculated with Eq. 5. The update to each cell consists of igniting the cell at random with probability p_{ij}, provided that the cell is not already on

fire. At the conclusion of the kth time step, we add the values from the newly computed M to the kth $n \times n$ matrix in M_{mean}. Once all simulations are completed, this summation of simulations per time step makes the following calculation straightforward:

$$M_{mean}(k) = \frac{1}{s} \sum_1^s M(k) \tag{7}$$

$M(k)$ and $M_{mean}(k)$ are the state of M in one simulation and the mean state of M respectively after the kth time step.

We verify the complete implementation of fire propagation by separately validating the effects of the two constituent influences of embers and wind. For a detailed discussion of our validation, refer to Section 6.

4 Results

For the results we show, we focus on studying the effects of varying ember cooling rate and wind magnitude for $p_0 < 0.5$, restricting our study to environments that are normally not conducive to fire propagation in the absence of embers and wind. We begin with a study of how embers and wind individually affect fire propagation qualitatively in Section 4.1 and quantitatively in Section 4.2 before proceeding to an analysis where we vary both d_0 and w in Section 4.3. For all results, we use the common parameters $a = 0.01$ and $p_0 = p_1 = 0.3$ and begin with one initial fire in the center of the matrix.

4.1 Initial Qualitative Results

Figure 3 shows a basic comparison of how introducing embers and wind as separate factors influences fire propagation. More specifically, Figure 3a demonstrates two simulations of fires at $t = 10, p_0 = 0.4$, both of which were evolved in the absence of wind to isolate the effect of embers. Both plots depict ignited cells as yellow and unlit cells as blue. The figure on the left displays the baseline scenario without embers, while the figure on the right propagates embers with $p_1 = 0.4, d_0 = 1$. For the last timestep, we observe that the area of the fire is roughly 8 times larger when embers are incorporated into the model. Visually, we see that cells at locations such as $(20, 20)$ and $(40, 50)$ are evidently not ignited when there are no embers, but are easily reached by the fire when embers are involved. Thus, we infer that embers do significantly increase the affected area of a fire for the given p_1, d_0.

It is also straightforward to see that the rate of fire propagation generally increases in Figure 3b, which shows $M_{mean}(t = 6)$ for $p_0 = 0.3$, $a = 0.01$, and three different choices of w and θ, but this increase occurs in the downwind direction instead. In producing these plots, we set $p_1 = 0$ to showcase the effect of wind only. The x and y axes indicate the positions of the cells within $M_{mean}(t = 6)$, and the yellow cells represent cells that have a value of approximately 1, while the dark blue cells represent cells that have a value of approximately 0. In all three cases, the highest fire values are concentrated in the center of $M_{mean}(t = 6)$, and we see that the fire generally propagates outward from the center cell in a radial manner. This result arises because we set the initial starting fire to be in the center, from which all successive fires are created. However, observe that while the area covered by fire is roughly circular in the leftmost plot, which involves no wind, the propagation of the fire is comparatively extended in a north-east direction in the middle plot, which involves a wind with $w = 40$ and $\theta = \frac{\pi}{3}$. Meanwhile, fire propagation extends directly south in the rightmost plot, which involves a wind with $w = 20$ and $\theta = -\frac{\pi}{2}$. This suggests that the presence of wind leads to an increased rate of fire propagation in the wind direction and, consequently, an increased mean area of fire coverage in that direction.

To offer a more structured comparison of different wind magnitudes w against different base probabilities p_0, we computed $M_{mean}(t = 6)$ for all possible $\{(p_0, w) \mid p_0 \in \{0.2, 0.3, 0.4\}, w \in \{0, 20, 40\}\}$. The nine resultant plots are displayed in Figure 4. In the figure, p_0 increases from top to bottom and w increases from left to right, and all cases were simulated with $p_1 = 0$ (no embers), $a = 0.01$, and $\theta = \frac{\pi}{3}$, indicating a general northeast direction for the wind. As seen most clearly in the left column, which involves no wind, increases in p_0 are associated with increases in the mean values of cells that occur in an evenly radial manner. This is evidenced by the greater number of nonzero cells distributed
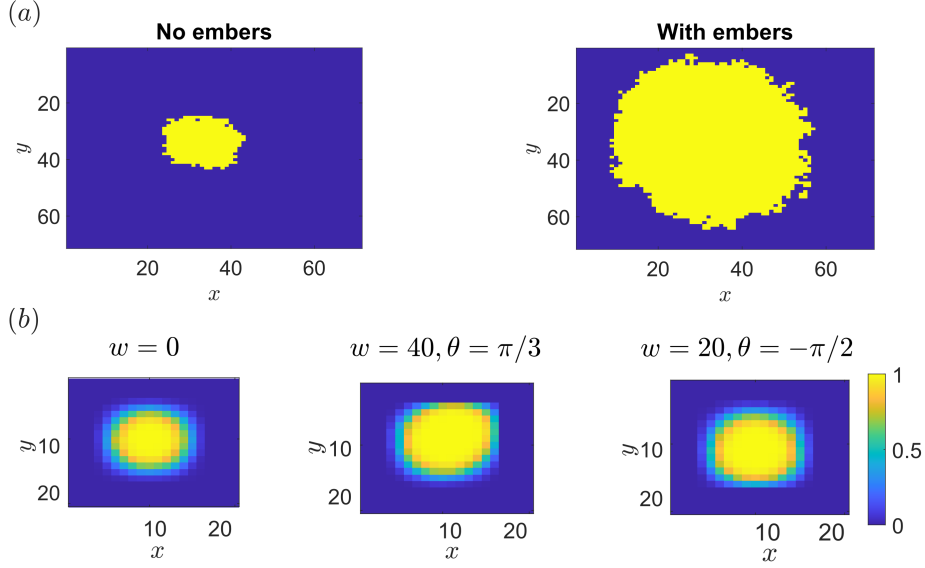
Figure 3: Qualitative results for ember-based ($w = 0$) and wind-based ($p_1 = 0$) simulations.
(a) One simulation of fire propagation without embers (left) and with embers (right). Each grid element is depicted as an individual pixel. Pixels in blue are not on fire, while pixels in yellow are. Both diagrams show the effect at $t = 10$ with $p_0 = p_1 = 0.4, d_0 = 1$. We observe the yellow region (i.e., the region on fire) is about 8x larger for the simulation with embers than the baseline simulation, which suggests embers can have a substantial capacity to increase wildfire size.
(b) Comparison of $M_{mean}(t = 6)$ for three different choices of w and θ, where the leftmost case involves no wind, the middle case imposes a wind with $w = 40$ and $\theta = \frac{\pi}{3}$, and the rightmost case imposes a wind with $w = 20$ and $\theta = -\frac{\pi}{2}$. Observe how the presence of wind is associated with increased fire propagation in the direction of the wind.

in all directions and further away from the center for higher p_0. In contrast, for each shown selection of p_0, increases in w are associated with increases in the mean values of cells that are restricted to the direction of the wind. We can see that the distribution of nonzero cells increases only in the northeast direction as w increases, leaving the values of cells unchanged in other directions and leading to an increasingly elliptical shape for the mean area covered by fire. The implication that an increase in wind magnitude visibly increases the rate of fire propagation only in the downwind direction for various $p_0 < 0.5$ is consistent with what we inferred from Figure 3.

We note an additional observation that for sufficiently low p_0, for which the original area covered by fire is smaller when there is no wind, there is an increased potential extent of the area covered by fire that follows from the increased rate of fire propagation in the downwind direction. To see this, observe that as w increases for $p_0 = 0.2$, the total extent of all cells affected by fire propagation clearly increases in the northeast direction, so the area affected is distinctly elliptical. The fire does not ever reach a cell such as $(4, 16)$ for $w = 0$, but can do so for $w = 40$, as shown by a lightened shade of blue for that cell. This implies that the possibility of that cell catching fire is introduced when the magnitude of the wind is sufficiently high. For $p_0 = 0.4$ and $p_0 = 0.6$, the effect of increasing wind magnitude is increasingly limited to changes in mean fire values across the original extent of the fire propagation, seen by changes in color, rather than an increased possible extent in the downwind direction. For these cases, few cells that are not affected by fire when $w = 0$ become possibly affected when $w > 0$.

4.2 Initial Quantitative Results

Visualizations of individual quantitative results for embers and wind are provided in Figure 5. Figure 5a shows the effect of increasing p_1 and d_0 for the increase in fire propagation r_c without considering wind for $t = 10$. Regions in blue show a small increase, while regions in yellow show an increase of 10x or large. We observe that for $d_0 > -0.47p_1 + 1.31$ (as defined by the red dotted line) we observe a significant increase (i.e., the yellow region).
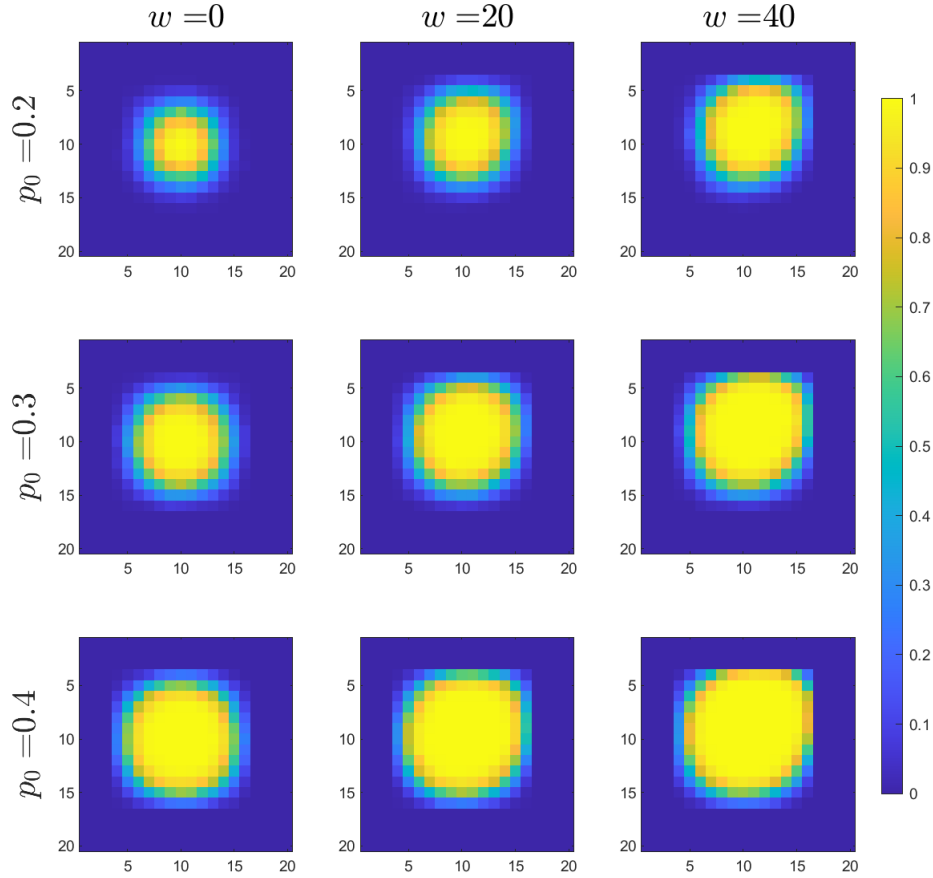
Figure 4: Comparison of $M_{mean}(t = 6)$ for three wind magnitudes w that increase from left to right ($w = 0, w = 20, w = 40$) and three base probabilities p_0 that increase from top to bottom ($p_0 = 0.2, p_0 = 0.3, p_0 = 0.4$), resulting in nine total cases for a further study of wind's effects. For all shown values of p_0, successive increases in w result in an increased average rate of fire propagation in the downwind direction.

To see why this is the case, recall from Section 2.2 that for increasing p_1, more embers emanate from a given cell. This, in turn, leads to an increase in the ignition probability $f(d)$ and, correspondingly, r_c. Similarly, for increasing d_0, embers remain warm for a longer period of time, hence $f(d)$ decreases more slowly. It follows that r_c increases for increasing d_0. From this figure, we conclude that embers can have a significant effect on the area of the fire, even for only moderately large choices of p_1 and d_0. Thus, with enough embers and warmer environments, the fire grows at a much faster rate in all directions, resulting in a greatly magnified area.

Although the rate of fire propagation increases in a different manner for wind, it is easy to show that increases in wind magnitude can also noticeably increase the area of a fire. For $p_0 = 0.3$ and $a = 0.01$, by counting the number of cells with a mean value of at least 0.9 for $w = 0$, $w = 20$, and $w = 40$ over time, we obtain the data visualized in Figure 5b. We plot the evolution of the counts from $t = 0$ to $t = 6$ for each of the three values of w, producing a combined line graph. Early on, based on this measure, the state of the fire appears similar between the three choices of w. After two time steps, the difference in cells with a mean value of at least 0.9 is nonexistent between the cases of $w = 20$ and $w = 0$ and minimal between the cases of $w = 40$ and $w = 20$.

However, the data for later time steps reveals that there is an increasingly clear difference in the number of cells with a mean value of at least 0.9 between the three scenarios. In particular, by comparing the counts at the last time step $t = 6$, we find a difference of $50 - 34 = 16$ cells between the counts for $w = 20$ and $w = 0$ and a difference of $65 - 50 = 15$ cells between the counts for $w = 40$ and $w = 20$. In the figure, we can also visually ascertain that the differences in counts grow larger as time

passes, with the largest gaps between the three lines being observed for $t = 6$. We conclude that as w increases, the effects of increased wind magnitude in terms of the mean area of the fire become more apparent over time.
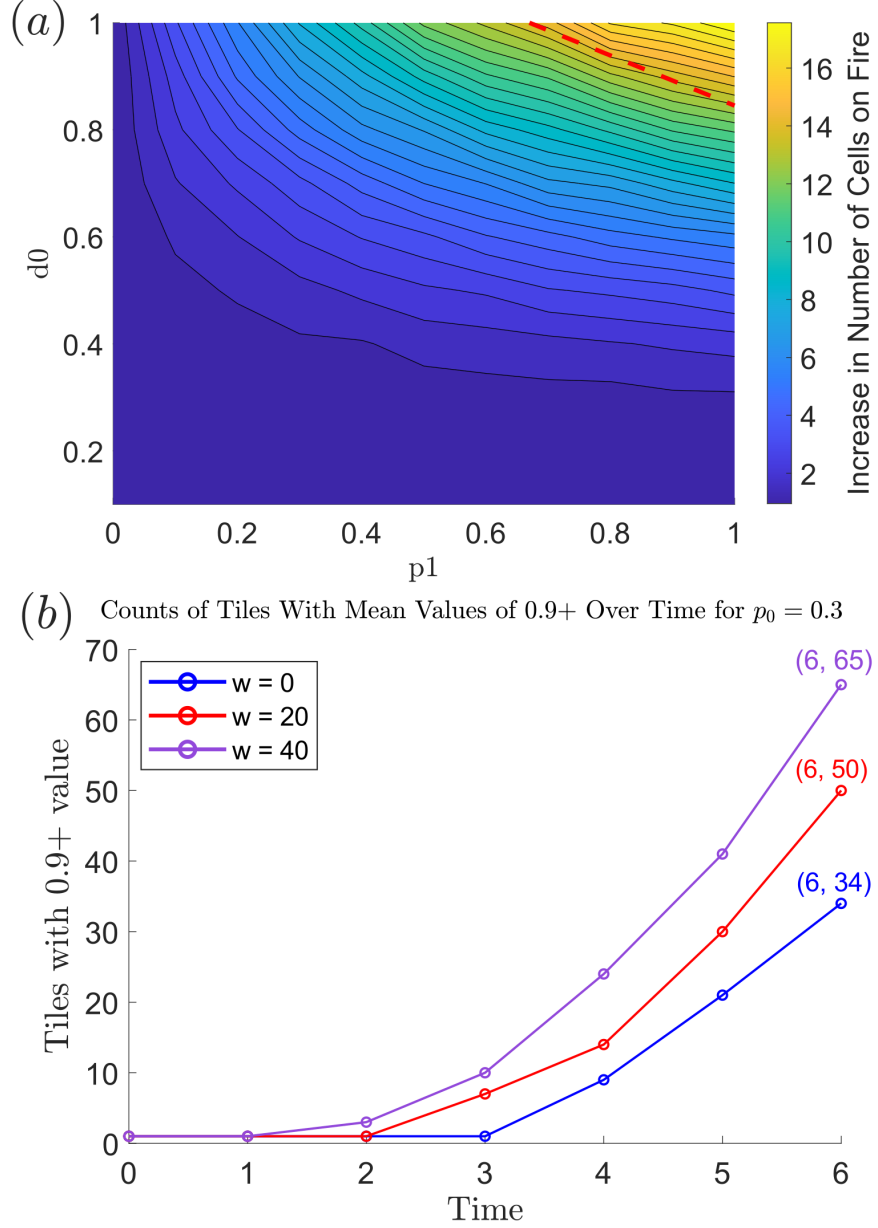

Figure 5: Quantitative results for ember-based ($w = 0$) and wind-based ($p_1 = 0$) simulations.
(a) Result for varying p_1 and d_0 ($0 \leq p_1 \leq 1$ and $0.1 \leq d_0 \leq 1$) with $t = 10$. The value of r_c is shown using a colormap, with blue representing low values and yellow representing large values. Notice that r_c is very high for increasing values of p_1, d_0. From the figure, it is obvious that $d_0 = -0.47p_1 + 1.31$ (the red dotted line) separates values of p_1, d_0 that have a very high r_c from those that do not.
(b) Comparison of number of cells with a mean value of $0.9+$ over six time steps for $w = 0$, $w = 20$, and $w = 40$, with $p = 0.3$ and all other parameters kept constant. Over time, the differences in the number of cells that have a mean value of at least 0.9 grow larger between the different values of w.

4.3 Combined Results

By running simulations for $\{(w, d_0) \mid w \in \{0, 10, 20\}, d_0 \in \{0.5, 1, 2\}\}$, we obtain the nine plots shown in Figure 6. These plots provide a comparison of mixing the effects of embers and wind together for

9

different choices of ember cooling rate and wind magnitude. As we increase w while holding d_0 constant, we see that there is an increased average rate of fire propagation in the downwind direction, towards which the fire fans out from the center of the matrix. As we increase d_0 while holding w constant, there is an increased average rate of fire propagation that is instead observed in all directions. These observations are consistent with what we found in Figures 2 and 4.

Note that for a low ember cooling rate, the effect of wind on fire propagation becomes less apparent. Studying $d_0 = 2$, we see that increasing w from 0 does not distend the shape of the area of the fire greatly from the original circular shape. In contrast, for $d_0 = 0.5$ and $d_0 = 1$, the area of the fire is clearly skewed much more strongly towards the wind direction than towards any other directions for larger w. This suggests that when the cooling rate is sufficiently low, the effect of the embers is so great that the additive effect from wind alters the rate of fire propagation in the wind direction minimally.

Figure 7 illustrates the effects of varying d_0 and w on the area of the fire for $t = 5$, as defined by the scaling ratio r_c. Regions that are cyan, green and yellow have a much larger fire relative to the baseline case without embers or wind, with $r_c \geq 10$. Unlike in 5a, we observe that the simulation only requires a relatively small w—around $w = 10$ and larger—to net a relatively large r_c (independent of d_0), with the fire becoming at least 10x larger. For the largest values of $(w, d_0) = (20, 2)$, we can observe a 30x increase in fire size, which is the largest increase we observe in our investigation. This provides compelling evidence that embers and wind together have massive potential in amplifying the area of a fire.
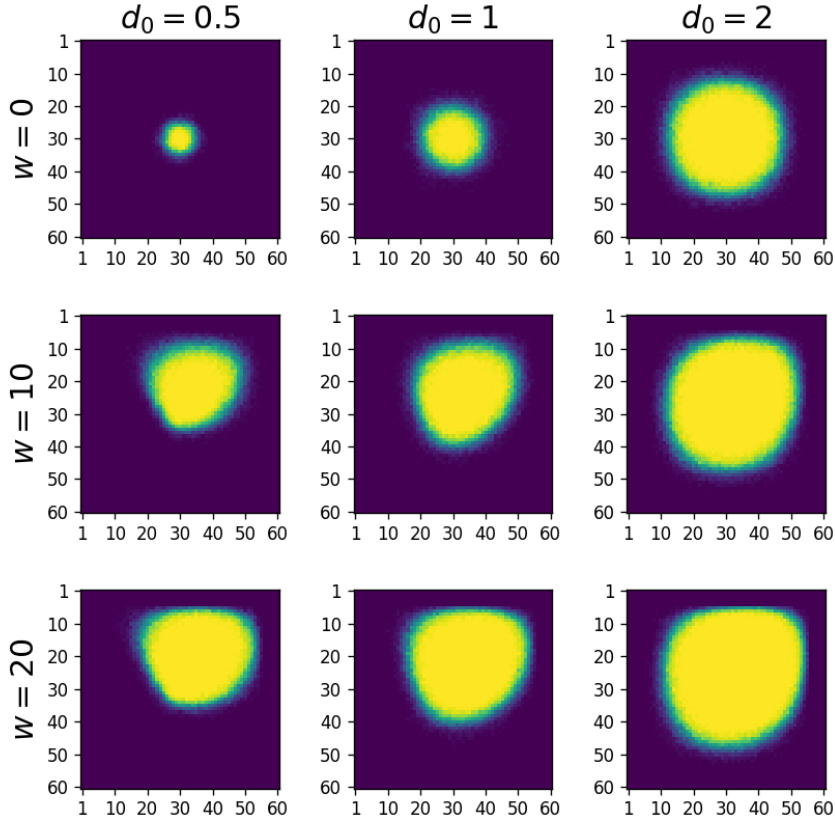

Figure 6: Comparison of $M_{mean}(t = 5)$ for three wind magnitudes w that increase from top to bottom ($w = 0, w = 10, w = 20$) and three distance factors d_0 that increase from left to right ($d_0 = 0.5, d_0 = 1, d_0 = 2$), resulting in nine total cases. For all shown values of d_0, successive increases in w result in an increased average rate of fire propagation in the downwind direction. Successive increases in d_0 also increase the rate of fire propagation, but this increase occurs in all directions, independent of θ.
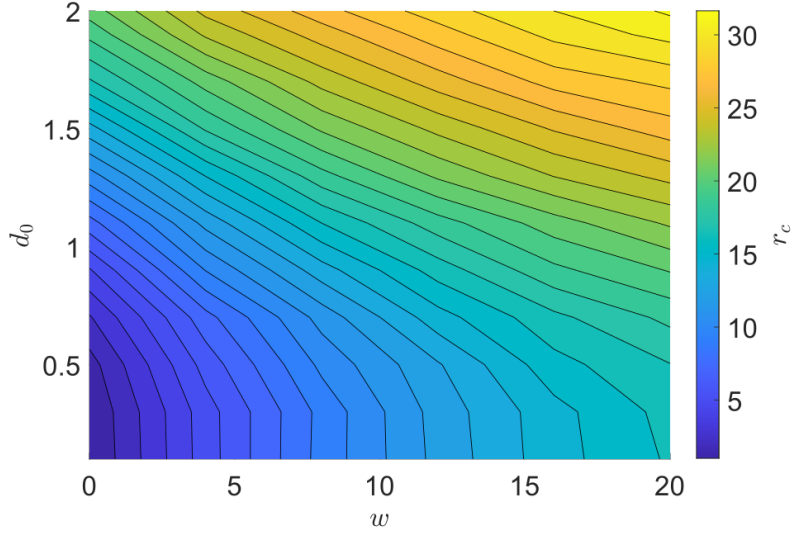
Figure 7: Colormap for r_c over a plot of d_0 vs. w for $0 < d_0 \leq 2$, $0 \leq w \leq 20$, and $t = 5$. Note that we set $p_0 = p_1 = 0.3$, $n = 60$, $t = 5$, $\theta = \frac{\pi}{3}$, $a = 0.01$ as constants. r_c increases both as d_0 increases and as w increases. However, the increase in r_c is most dramatic when both parameters are increased. We notice that for moderately large w (i.e., $w > 10$, corresponding to the cyan, green and yellow regions) we have at least a 10x increase for all d_0, which is practically significant.

5   Discussion

In summary, we have sought to determine how varying the properties of embers and wind impact the rate of wildfire propagation in environments that are otherwise unfavorable to such propagation. The results of our model suggest that increasing wind magnitude induces an accelerated rate of fire propagation in the general wind dire, resulting in an increased likelihood of fire propagation in that direction and, for particularly unfavorable environments, increasing the total possible extent of the area of fire spread. Furthermore, this effect accumulates over time while the presence of wind persists, causing the difference between the area covered by fire and the same defined area in the situation of reduced or nonexistent wind to become increasingly large.

Meanwhile, from figures 3a and 5a, we observe that the presence of embers also confers a significant effect on fire propagation, with up to an 18x increase in the area of the fire. This is important as even for relatively small ignition probabilities, embers have the capacity to amplify the rate of fire propagation greatly.

Combining wind and embers, we note that if embers cool down more slowly, the spread of the fire is more even, regardless of the wind strength w. From this, we suspect that the effects of embers are able to outpace the effects of wind. Nevertheless, we ultimately conclude that the two phenomena can work in tandem to significantly increase fire size to up to 30 times that of groundfire propagation. This factor of amplification is much greater than what we observe for either embers or wind alone.

While we have endeavored to construct a model that provides useful and accurate results, there are several ways that our model could be improved on to expand its utility. In defining our model, we made several ad-hoc decisions for the definitions of formulas and certain parameters. While we chose to model $f(d)$ with a decreasing exponential function, it would be interesting to consider other families of functions (e.g. hyperbolic, inverse trigonometric, etc.) from which alternative decreasing functions $f(d)$ could be derived. In addition, our choices of $d_{max} = 5$ and $a = 0.01$ were chosen in an ad-hoc manner. While the d_{max} we use is sufficient for our results because $f(d)$ for $d > 5$ is negligible for the values of d_0 and p_1 we study, this would not hold true for larger values of d_0 and/or p_1, in which case choosing some $d_{max} > 5$ would provide more accurate findings. There may also be better choices of a which would make our model more applicable to real-world scenarios. In fact, there is even potential to improve the form of Eq. 3 so that the natural variation of wind is captured more realistically. With reference to the roles of embers and wind, we conclude that there exist many possibilities for the future

improvement of this model.

Relatedly, by utilizing an arbitrarily chosen p_0 as a base probability of fire propagation that is augmented by the spread of embers and presence of wind, we have also not brought into consideration the plethora of other environmental factors that can influence fire propagation. We have introduced p_0 as a probability that is generally applicable when embers and wind are not considered. Additionally, p_0 is independent of direction and space, thereby providing us with an idealized scenario for our work. However, in the real world, the probability of fire propagation does vary with direction and space. For instance, there may be changes in elevation, where uphill and downhill travel affects the probability of propagation. Differences in the regional terrain can also expedite or impede wildfire growth. It is even known that sufficiently strong fires are capable of generating their own wind in addition to natural winds; we have not accounted for such types of wind in our model. Furthermore, our model fails to account for the finite nature of fires, which only last so long as fuel is available to sustain them. Future work is thus necessary to improve the presented model by including other significant environmental factors that are known to affect the rate of fire propagation.

Nonetheless, our current work provides a solid foundational model that helps to inform real-world scenarios in which considerable quantities of embers and/or strong winds play a major factor in the spread of wildfires. In particular, our model is highly applicable to relatively homogeneous regions and flat regions such as grasslands. While all wildfires start off small, we have found that embers and wind each have the potential to magnify the spread of a wildfire far beyond what would be expected in an environment that may otherwise not be conducive to rapid fire propagation. The united effect of embers that are carried by winds is even more powerful. This dangerous combination can separate a fire that dies out quickly from a fire that grows to an uncontrollable size, causing significant damage to the surrounding landscape. As such, it is critically important to pay heed to the effects of embers and wind factors, so as to minimize the destructive impact of future wildfires.

6 Appendix I: Method Validation

6.1 Embers validation

To test the validity of our model implementation in computing the influence of embers, we set $w = 0$ and perform $s = 100,000$ simulations of the first time step from an 11×11 matrix with one cell ignited in the center and take the average of the resulting matrices. We refer to this mean matrix after the first time step as M_1. Around the center of M_1, we expect the surrounding values to correspond well with the value of $f(d)$ for each cell. To measure the relative error, we take the value of each cell $M_1(i,j)$ and compute the relative difference Δm_1 from $f(d)$:

$$\Delta m_1 = \frac{|M_1(i,j) - f(d)|}{f(d)} \tag{8}$$

Using Eq. 8, we obtain the visualized relative error for M_1 in Figure 8. In the figure, cells close to the center have a trivial relative difference, as shown by the concentrated dark purple color. Meanwhile, cells further away have an error of around 10%. However, a few cells that are a distance greater than 4 away from the center have errors at or over 50%. This is most likely due to distant cells having a very low ignition probability, suggesting that we would need to average far more simulations for the error in these cells to converge to 0. Still, the low error we observe for a clear majority of cells, particularly those that do not form the border of the matrix, demonstrates that we can be reasonably confident about the accuracy of our implementation of embers.
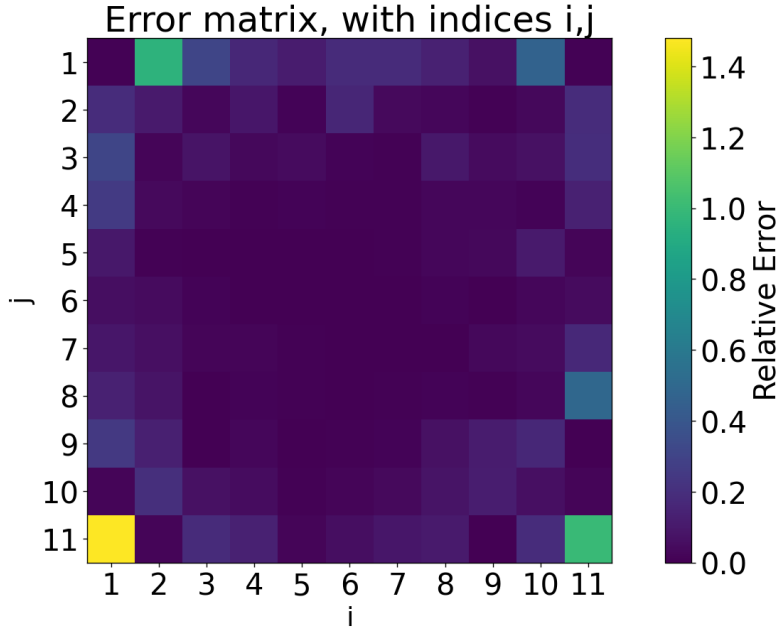

Figure 8: Relative error over 100,000 runs with $n = 11, p_1 = 0.5, d_0 = 0.6$. Dark purple cells have low error, while bright yellow cells have high error. Cells close to the center have very low error, whereas distant cells have high error (> 0.5), most likely due to the limits of the random number generator and the very small probabilities computed for large d.

6.2 Wind validation

If we decouple our model implementation of wind from our implementation of embers by setting $p_1 = 0$, then we only need to verify that the cells adjacent to fires correspond to the respective $K(i,j) = p_0 + W(i,j)$, meaning that we can use smaller n for our validation of wind. We provide two cases for this validation over a single time step, for which we list the analytical calculations and expected results.

13

We introduce a simple case for validation first. Given $p_0 = 0.3$, $w = 20$, $\theta = \frac{\pi}{3}$, $a = 0.01$, and one initial fire in the center of a 3×3 matrix, we have $\boldsymbol{w_{xy}} = \left[20cos(\frac{\pi}{3}); 20sin(\frac{\pi}{3})\right] = [10; 17.3205]$. Running a single time step over many simulations should yield mean values of approximately

- $p_0 + a\frac{(\boldsymbol{w_{xy}} \cdot [-1;1])}{||[-1;1]||} = 0.3518$ for the cell at $(1, 3)$,

- $p_0 + a\frac{(\boldsymbol{w_{xy}} \cdot [0;1])}{||[0;1]||} = 0.4732$ for the cell at $(1, 2)$,

- $p_0 + a\frac{(\boldsymbol{w_{xy}} \cdot [1;1])}{||[1;1]||} = 0.4932$ for the cell at $(1, 3)$,

- $p_0 + a\frac{(\boldsymbol{w_{xy}} \cdot [1;0])}{||[1;0]||} = 0.4$ for the cell at $(2, 3)$,

- $p_0 + 0 = 0.3$ for all other neighboring cells,

- and 1 for the center cell at $(2, 2)$.

Again, let M_1 represent the mean matrix after one time step over $s = 100,000$ simulations. Let $M_{expected}$ represent the expected results listed above. Then the relative error m_2 between M_1 and $M_{expected}$ for each cell is

$$\Delta m_2 = \frac{|M_1(i, j) - M_{expected}(i, j)|}{M_{expected}(i, j)} \tag{9}$$

Figure 9 plots this relative error, where dark blue indicates an error close to 0 and yellow indicates a higher error close to 0.01. We see that all relative errors per cell are easily less than 0.01, demonstrating that our implementation is valid for this set of parameters.
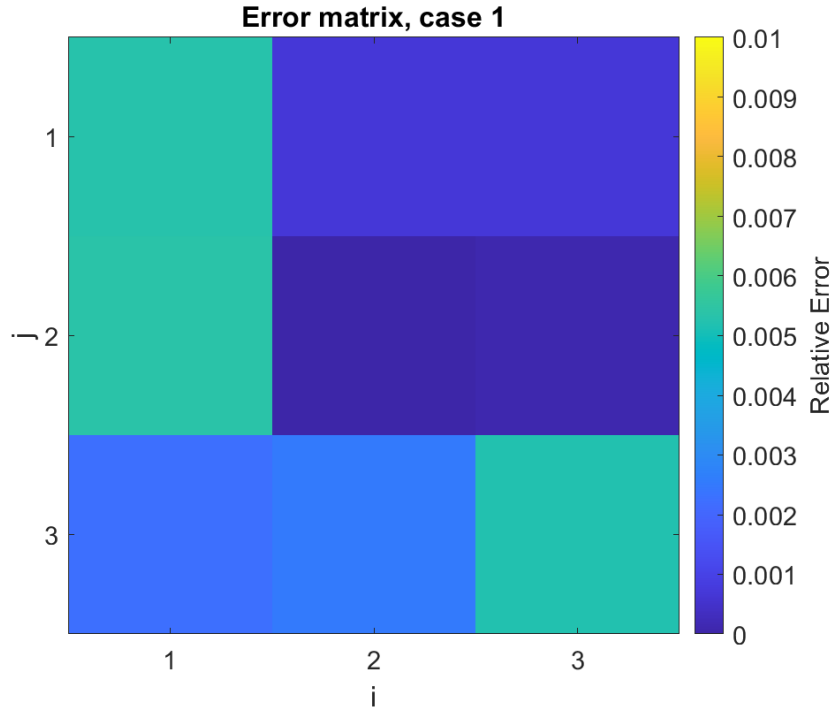

Figure 9: Relative error over 100,000 runs for one time step for $n = 3$, $p_0 = 0.3$, $w = 20$, and an initial fire at $(2, 2)$, where dark blue corresponds to a low error and bright yellow corresponds to a higher error of up to 0.01. Note that the relative error is less than 0.01 for all cells, providing compelling evidence for the validity of our implementation.

We now present a more complex case to validate. Given $p_0 = 0.3$, $w = 20$, $\theta = \frac{\pi}{3}$, $a = 0.01$, and four initial fires in the center of a 6×6 matrix, we still have $\boldsymbol{w_{xy}} = \left[20cos(\frac{\pi}{3}); 20sin(\frac{\pi}{3})\right] = [10; 17.3205]$. Running a single time step over many simulations should yield a mean value of 0 for all cells that form the outer border of the matrix. For the cells within the border, we should have

- $1 - (1 - p_0 - a\frac{(\boldsymbol{w_{xy}} \cdot [-1;1])}{||[-1;1]||}) = 0.3518$ for the cell at $(2,2)$;

- $1 - [(1 - p_0 - a\frac{(\boldsymbol{w_{xy}} \cdot [0;1])}{||[0;1]||})(1 - p_0 - a\frac{(\boldsymbol{w_{xy}} \cdot [-1;1])}{||[-1;1]||})] = 0.6585$ for the cell at $(2,3)$;

- $1 - [(1 - p_0 - a\frac{(\boldsymbol{w_{xy}} \cdot [0;1])}{||[0;1]||})(1 - p_0 - a\frac{(\boldsymbol{w_{xy}} \cdot [1;1])}{||[1;1]||})] = 0.7330$ for the cell at $(2,4)$;

- $p_0 + a\frac{(\boldsymbol{w_{xy}} \cdot [1;1])}{||[1;1]||} = 0.4932$ for the cell at $(2,5)$;

- $1 - [(1 - p_0 - a\frac{(\boldsymbol{w_{xy}} \cdot [-1;1])}{||[-1;1]||})(1 - p_0)] = 0.5462$ for the cell at $(3,2)$;

- $1 - [(1 - p_0 - a\frac{(\boldsymbol{w_{xy}} \cdot [1;0])}{||[1;0]||})(1 - p_0 - a\frac{(\boldsymbol{w_{xy}} \cdot [1;1])}{||[1;1]||})] = 0.6959$ for the cell at $(3,5)$;

- $2p_0 - p_0^2 = 0.51$ for the cells at $(4,2)$, $(5,3)$, and $(5,4)$;

- $1 - [(1 - p_0 - a\frac{(\boldsymbol{w_{xy}} \cdot [1;0])}{||[1;0]||})(1 - p_0)] = 0.58$ for the cell at $(4,5)$;

- $p_0 + 0 = 0.3$ for the cells at $(5,2)$ and $(5,5)$;

- and 1 for the center four cells at $(3,3)$, $(3,4)$, $(4,3)$, and $(4,4)$.

As with the simple case, we provide a visualization of the relative error calculated with Eq. 9 in Figure 10. Again, we see that the relative error for each cell is clearly less than 0.01, providing strong evidence for the validity of our wind implementation and the results that we draw from it.
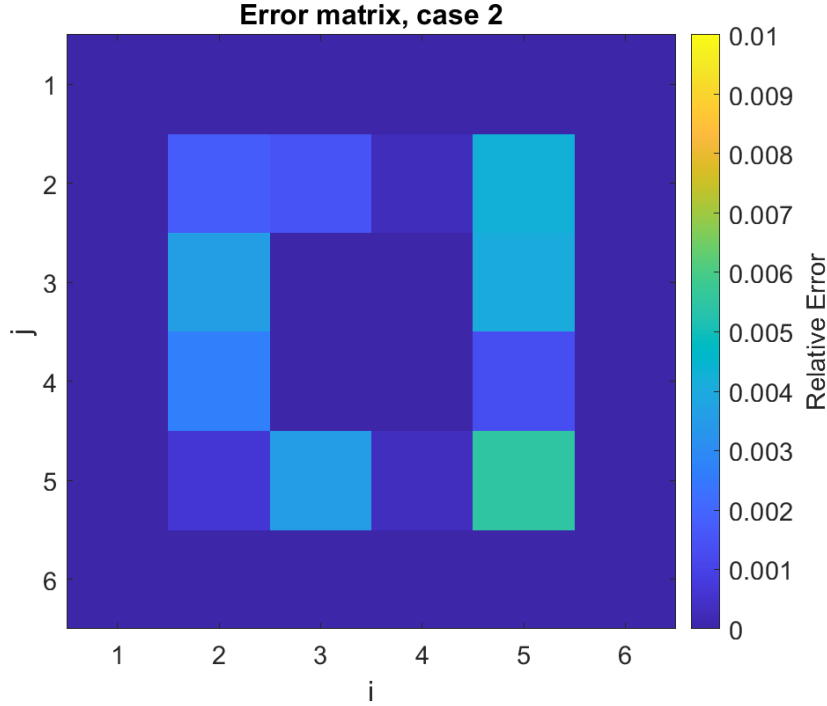

Figure 10: Relative error over 100,000 runs for one time step for $n = 6$, $p_0 = 0.3$, $w = 20$, and initial fires at $(3,3)$, $(3,4)$, $(4,3)$, and $(4,4)$, where dark blue corresponds to low error and bright yellow corresponds to high error. Once again, the relative error is less than 0.01 for all cells, giving further evidence for the validity of our implementation.

References

[1] F. W. Defense, "California Wildfires History & Statistics | Frontline Wildfire Defense," Sep. 2020. [Online]. Available: https://www.frontlinewildfire.com/wildfire-news-and-resources/california-wildfires-history-statistics/

[2] 9NEWS, "What causes homes to catch fire during a wildfire?" Dec. 2021. [Online]. Available: https://www.youtube.com/watch?v=bWtYtqADmqU

[3] "Definition of EMBER," Mar. 2024. [Online]. Available: https://www.merriam-webster.com/dictionary/ember

[4] "Marshall fire started by week-old embers on Twelve Tribes property, sparking Xcel power line, Boulder sheriff says," Jun. 2023. [Online]. Available: https://www.fortmorgantimes.com/2023/06/08/marshall-fire-cause-origina-investigation-boulder-colorado/

[5] "California Witch and Guejito WUI Fires 2007," *NIST*, Jun. 2011, last Modified: 2017-01-06T10:44-05:00. [Online]. Available: https://www.nist.gov/el/california-witch-and-guejito-wui-fires-2007